Strain and Temperature Modulated Growth of Mn_3Ga Films

Dennis J. X. Lin,[1]* B. C. Lim,[1]* Hnin Yu Yu Ko,[1] Nelson C. B. Lim,[1] Henry Y. L. Lee,[1] Hang Khume Tan,[1] Royston J. J. Lim,[1] Shaohai Chen,[1†] Pin Ho[1†]

*[1] Institute of Materials Research & Engineering, Agency for Science, Technology & Research (A*STAR), Singapore 138634*

** denotes equal author contributions*
† denotes corresponding authors
Email: hopin@imre.a-star.edu.sg; chen_shaohai@imre.a-star.edu.sg

Abstract

Antiferromagnetic (AF) and ferrimagnetic (FiM) thin films have demonstrable burgeoning significance to prospective spintronics applications. From the idiosyncrasy in parasitic stray field mitigation to ultrafast low power switching, this underpins felicitous properties for incorporating AF and FiM films in functional memory and computing devices. Mn_3Ga adaptably features a multitude of spin orders that can be meticulously controlled with stoichiometry, temperature, and strain modulations. In this work, we have carefully designed three suitable stacks of Mn_3Ga thin films on single crystal MgO, STO and STO/Ta substrates deposited across varying substrates temperature. The delicate interplay of strain and temperature tuning is examined by characterizing their magnetic, crystallographic, and morphological properties. Their non-directional magnetic anisotropy and saturation magnetization coincide well with corresponding tetragonal FiM and hexagonal AF Mn_3Ga phases. Importantly, we observed that STO strain-regulated tetragonal phase is stabilized over a larger temperature window and provides more compact, uniformly sized granular growth. This work establishes a sturdy methodology in understanding Mn_3Ga thin film growth for eventual AF and FiM-based memory and computing applications.

Introduction

Ferrimagnetic (FiM) and antiferromagnetic (AF) materials have garnered great interest in the last decades for their potential applications in next generation spintronics[1-5](1-5). Conventionally, the neighboring spins of FiM and AF materials align in a collinear antiparallel configuration with partially and fully compensated magnetic moments, respectively[6]. Their negligible net magnetic stray fields and robustness to external magnetic field perturbation[7-10] make them ideal building blocks for scalable and energy-efficient logic, memory, and computing devices[3, 4, 11, 12]. In addition, building on their terahertz spin dynamic responses, FiM and AF materials are also promising in realizing ultrafast switching and data processing. Amongst the plethora of FiM and AF material systems, research on the Mn_3X family (X = Sn, Ge, Ga, Ir, Pt, Rh) with unconventional non-collinear, triangular spin arrangements have gained traction due to recent discoveries of room-temperature detection mechanisms such as large anomalous hall effect and magnetoresistance, and electrical manipulation of magnetic orders at terahertz scale[4, 5, 9-11, 13-19]. In particular, Mn_3Ga is an attractive candidate due to its rich crystal structures and associated magnetic orderings – $D0_3$ face centered-cubic (*fcc*) lattice displaying collinear AF order, $D0_{22}$ tetragonal (τ) lattice with tunable FiM and FM orders depending on its Mn-Mn interatomic spacing, and $D0_{19}$ hexagonal (ε) lattice exhibiting non-collinear AF order[3, 5, 10-12, 18, 20-23].

To tune the magnetic textures and properties of Mn_3Ga material system[12, 20], early work has demonstrated viable means of modulating substrate straining, annealing temperatures and buffer layers. Phenomenologically, lattice strain and temperature define critical parameters of surface energetics and thermodynamics which influence the texture and morphology of Mn_3Ga crystals. By engineering the strain of Mn_3Ga film grown on Si, MgO (111), GaN (001) and MgO (001)/Pt (111) substrates, the extent of canting of Mn magnetic moments along the *c*-axis can be controlled to achieve varying magnetic properites[21]. Meanwhile, annealing plays a key role in determining the Mn_3Ga crystallographic structure, wherein τ-Mn_3Ga structure can evolve to cubic $L1_0$ while disordered-cubic to ordered-cubic $L1_2$-Mn_3Ga with increasing annealing temperatures[20]. Further, utilizing various buffer layers including Ta, Pt and Cr lead to different film characteristics such as pinholes concentration and roughness, influencing the morphology and orientation of the Mn_3Ga thin films through different growth modes[12].

Till date, studies have focused on MgO substrates due to their small lattice mismatch with τ-Mn_3Ga[12, 20, 21]. In our experiment, by depositing Mn_3Ga films on MgO (111) and $SrTiO_3$ (STO) (111) substrates, and by varying the substrate temperature (T_s), we established a foundation in Mn_3Ga thin film structural growth methodology that consists of τ- and ε-Mn_3Ga phases. The magnetic and crystal texture studies show that with a high T_s, the τ-Mn_3Ga or ε-Mn_3Ga phases can be obtained on both substrates. While in morphology study, it is found that the Mn_3Ga film grown on STO substrate possesses a more uniform granular structure. These results will provide insights on the utilization of Mn_3Ga material platform for diverse spintronics applications.

Methods

Three sample stacks consisting MgO/Mn_3Ga(25)/Pt(5), STO/Mn_3Ga(25)/Pt(5) and STO/Ta(3)/Mn_3Ga(25)/Pt(5) were deposited. The numbers in parentheses are in nm. For simplicity, the three stacks are henceforth referred to as MgO, STO and STO/Ta, respectively. The multilayers were deposited on single crystal STO (111) and MgO (111) substrates by using a Chiron™ ultra-high vacuum sputtering system. To obtain the Mn_3Ga layer, a composite target consisting of Mn 75% and Ga 25% was used. The Mn_3Ga and the Ta layers were deposited at varying substrate temperatures (T_s) of room temperature (RT), 200, 400 and 500 ºC,

respectively. All Pt layers were deposited at RT. The magnetic properties were characterized using alternating gradient force magnetometry (AGM, Micromag™). The crystal structures and lattice parameters were determined with x-ray diffraction (XRD, Bruker™ D8 Discoverer) using Cu K_α radiation. Atomic force microscopy (AFM, Bruker™ Dimension 3100) was utilized for surface roughness measurements. The scan size, scan rate, and lift height used were 5 x 5 um, 1 Hz, and 30 nm respectively. The surface morphology and grain size distribution were examined using scanning electron microscope (SEM, Hitachi™ SU8220) operated at 5kV to further validate and ascertain key characteristics of grain size and its corresponding distributions. All measurements were performed at RT.

Results & Discussion

First, we posit that the lattice mismatch arising from MgO (111) and STO (111) substrates will influence the Mn_3Ga crystallographic texture. Figure 1a-b demonstrate the τ-Mn_3Ga structure with respect to the non-uniaxial straining directions of MgO (111) and STO (111) substrates, respectively. On <111> substrate surface, there exist two sets of family directions namely [110] and [211] that are expected to imbue a favorable straining interface compatibly. Given the theoretical τ–Mn_3Ga lattice constants of a = 3.771 Å and c = 6.881 Å, the lattice mismatch is approximated to be 10.55 % along [110], 3.29 % along [211] for MgO and 3.61 % along [110], 7.26 % along [211]. This suggests that the film will be preferentially oriented at 45° i.e. [110] direction of film rests upon [110] and [211] directions of the substrate. As such, even with epitaxial growth, we expect that the FiM or AF τ-Mn_3Ga film deposited on MgO (111) and STO (110) substrates will not exhibit complete out-of-plane magnetic anisotropy i.e., easy axis along the [001] direction[23].

In Figure 2a-c, the top and bottom panels reveal the key magnetic parameters of in-plane (IP) and out-of-plane (OP) saturation magnetization (M_s) and coercive field (H_c) of the MgO, STO and STO/Ta samples across different T_s. The M_s dependence of T_s for both MgO and STO samples (Fig. 2a, b) show an exponential increase with increasing T_s, e.g. the IP and OP M_s of the STO samples increase from ~20 to 60 and 10 to 45 kA/m, respectively. The values at high T_s suggests FiM orderings relatable range-wise to reported IP Ms values[12, 20]Additionally, their $M(H)$ loops (Fig. 2a, b insets) also suggest no preferential IP or OP anisotropy, corroborating well with the expected [110] orientation (Fig. 1). In contrast, the M_s of the STO/Ta stack is relatively constant at ~15 kA/m across different T_s (Fig. 2c) as the strain-induced effect of the STO substrate is disrupted by the Ta buffer layer. Meanwhile, in all 3 sets, we observed a larger OP than IP H_c which remain relatively constant across varying T_s. Such magnetic properties may be attributed to crystal structures, grain formation and grain size distributions which will be subsequently discussed.

The XRD spectra were characterized to understand the texture variation of Mn_3Ga grown on the MgO, STO and STO/Ta (Fig. 3a-c). For the MgO stack, the signature MgO (111) peak at 39.70° overlaps with the *fcc*-Mn_3Ga (110) peak at T_s = RT. Increasing T_s to 200 °C leads to the emergence of a relatively broad τ-Mn_3Ga (112) peak at 42.12°, constituting the onset of τ phase. At T_s = 400 °C, a secondary τ-Mn_3Ga (111) peak at 41.42° appears together with the neighbouring τ-Mn_3Ga (112) peak, suggesting that the observed 42.12 ° peak at T_s = 200 °C is a superimposed of both characteristic τ-Mn_3Ga peaks. Further increase in T_s to 500 °C results in the emergence of ε-Mn_3Ga (200) phase at 40.46°, coexisting with a weak presence of τ-Mn_3Ga (111) phase. In contrast, the STO stack shows an onset of τ-Mn_3Ga (112) phase at T_s = 200 °C and evolved to the τ-dominated (111) and (112) phase at T_s = 500 °C, albeit with additional ε-Mn_3Ga (002) and (201) peaks at T_s = 400°C. The presence of FiM τ-Mn_3Ga (111) phases in both MgO and STO stacks at higher T_s could possibly contribute to the increasingly

larger M_s. Additionally, the stark difference in the stabilization temperature window of τ-phase retention signifies a strain associated enhancement characteristic exclusive to STO. In STO/Ta stack, the τ and ε-phase emerge simultaneously as a mixed phase with increasing T_s up to 500°C, which is in line with our previous results[23].

The lattice parameters a and c of the three sets of samples are derived using Bragg's law and summarized in Fig. 3d-f. The analysis here will focus on the strain-induced effect of MgO and STO (111) on the τ- and ε- phases, omitting *fcc*-Mn_3Ga as the pronounced mismatch on <111> is energetically unfavourable for its formation. For the MgO stacks, the lattice parameters of Mn_3Ga are obtained as a = 4.86 Å and c = 6.07 Å for the τ- phase at T_s = 200 and 400 °C, and a = 5.14 Å and c = 3.87 Å upon formation of the ε-phase at T_s = 500 °C. Meanwhile, the lattice parameters of the STO and STO/Ta stacks are found to be relatively constant at a = 4.85 (5.60) Å and c = 6.07 (4.04) Å for the τ-(ε-) phase across all the T_s. The lattice parameters of τ–phase disclose a prominent deviation from the theoretical values of a = 3.77 Å and c = 6.88 Å, suggesting that the <111>-induced strain has effectively applied a tensile-like planar distortion to expand the intrinsic Mn_3Ga lattice. Furthermore, the lateral growth of the c-axis (c ~ 6.070 Å) of the τ–phase is feasibly along the <111> substrate, resulting in non-uniaxial anisotropy consisting of both IP and OP components (Fig 2a-b insets).

To further understand the influence of the substrates and T_s on the Mn_3Ga film growth mode, we inspected the morphological evolution of the three sets of stacks. The root-mean-square roughness (R_q) variation and the representative AFM images of the three sets of stacks are shown in Fig. 4a-c. Similar R_q-T_s trend is observed across the MgO and STO stacks, wherein the R_q maintains a near-constant value of ~2 nm at $T_s \leq$ 200 °C and increases drastically to ~12-15 nm at T_s = 500 °C. In contrast, the R_q for the STO/Ta stack adopts a linear increase from ~1 to ~12nm with increasing T_s from RT to 500°C. For all three sets of stacks, the Mn_3Ga film growth evolves from a uniform conformal coverage at RT to a granular polycrystal at high T_s. This is understandable as the nucleation rate with number of sites follows the Arrhenius relation[24] closely, as well as the elevated temperature also favors kinetic motions.

Finally, we focus on examining the SEM images and the corresponding grain size (d) distribution of the τ-Mn_3Ga dominant films at T_s = 400°C (Fig. 4d-f). Evidently, the τ-Mn_3Ga growth on STO exists as largely compactified, normally distributed grains (mean grains, $d_{ave} \approx$ 100nm) in contrast to the rugged coalescent growth of higher grain dispersity on MgO. These imply that the strain-induced heteroepitaxial growth can alter the size distribution of both stacks. In the STO/Ta stack, the Mn_3Ga film shows an extremely sporadic, incoherent coverage and randomly dispersed grains of d < 80 nm. Since the Ta buffer layer is expected to release the induced strain, the granularity of the STO/Ta stack may instead be ascribed to the inhomogeneity of Ta surface energy at high temperatures[23]. The most preferred crystallites/grain structures would be the strain induced STO, in accordance with extent of granularity, compactness and uniformity relative to its size dispersity.

Conclusion

In summary, we have sequentially examined three sets of strain attuned Mn_3Ga thin films on respective single crystal MgO (111), STO (111) substrates and Ta buffer. With the substrate temperature T_s ranging from RT to 500°C, the Mn_3Ga films, without uni-directional anisotropy, shows increasing or relatively constant M_s when deposited on single crystal substrates or Ta buffer, respectively. The M_s variation of both MgO and STO stacks coincides with the emergence of the Mn_3Ga τ-phase when T_s >200 °C. Compare with using MgO substrate, the Mn_3Ga *s*tructural ramifications under STO confined strain have alluded to strain-enhanced

phenomena of τ-preferential stabilization. On the other hand, the morphology studies show that the grains of all Mn_3Ga film transformed from uniform coverage to discrete granular-like polycrystals with increasing T_s. At T_s = 400 ºC, both the MgO and STO stack show larger granular size than the STO/Ta stack. Overall, our results demonstrate that the substrates have direct influence on the modulation of phase and their associated transition temperatures. This set a precedent in establishing robust growth methodologies of Mn_3Ga to acquire the desired structural and surface properties through the combined utilization of precise stoichiometry, thermal and strain tuning, facilitating further characterization techniques that require delicate balancing of film properties.

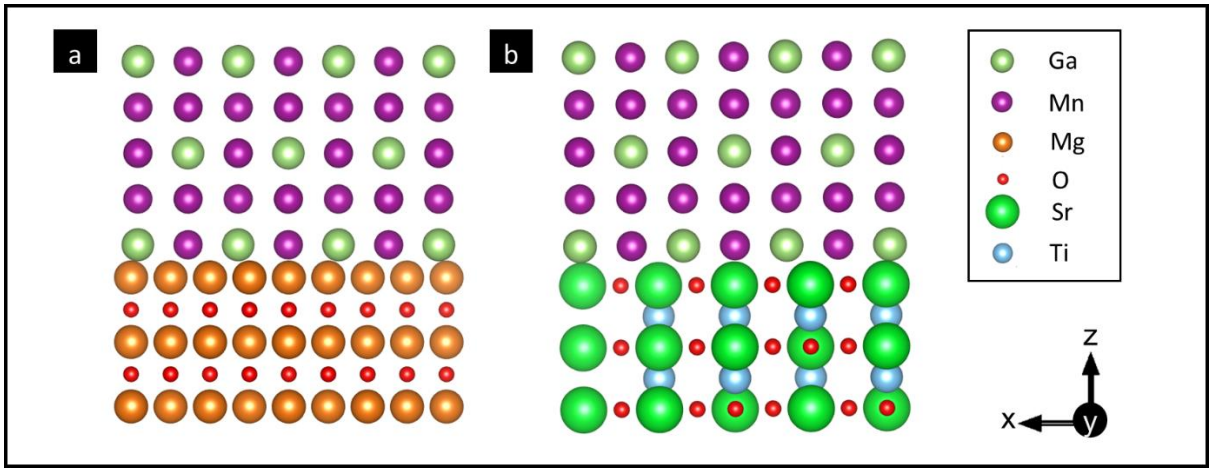

Figure 1. Schematic of τ-Mn3Ga (001) grown on a) MgO (111) and b) STO (111) substrate.

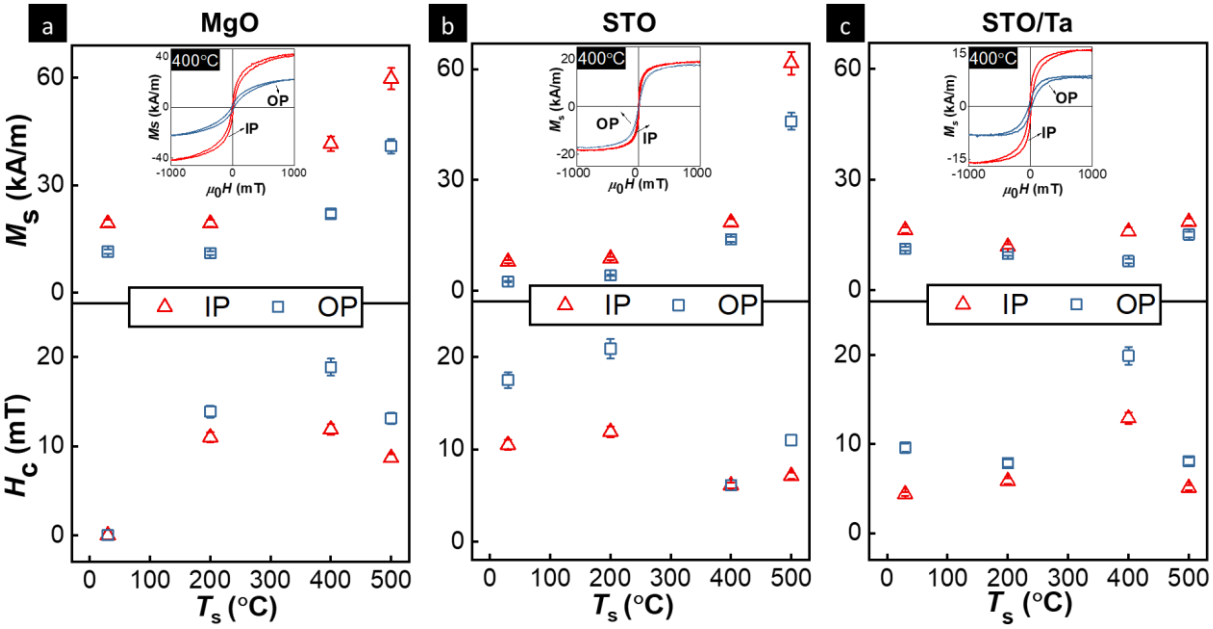

Figure 2. M_s (top) and H_c (bottom) of Mn3Ga thin films on a) MgO substrate b) STO substrate and c) STO substrate with Ta buffer layer at T_s of RT, 200 ºC, 400 ºC and 500 ºC. Insets show M-H loop of corresponding substrate with 25 nm Mn3Ga at 400 ºC.

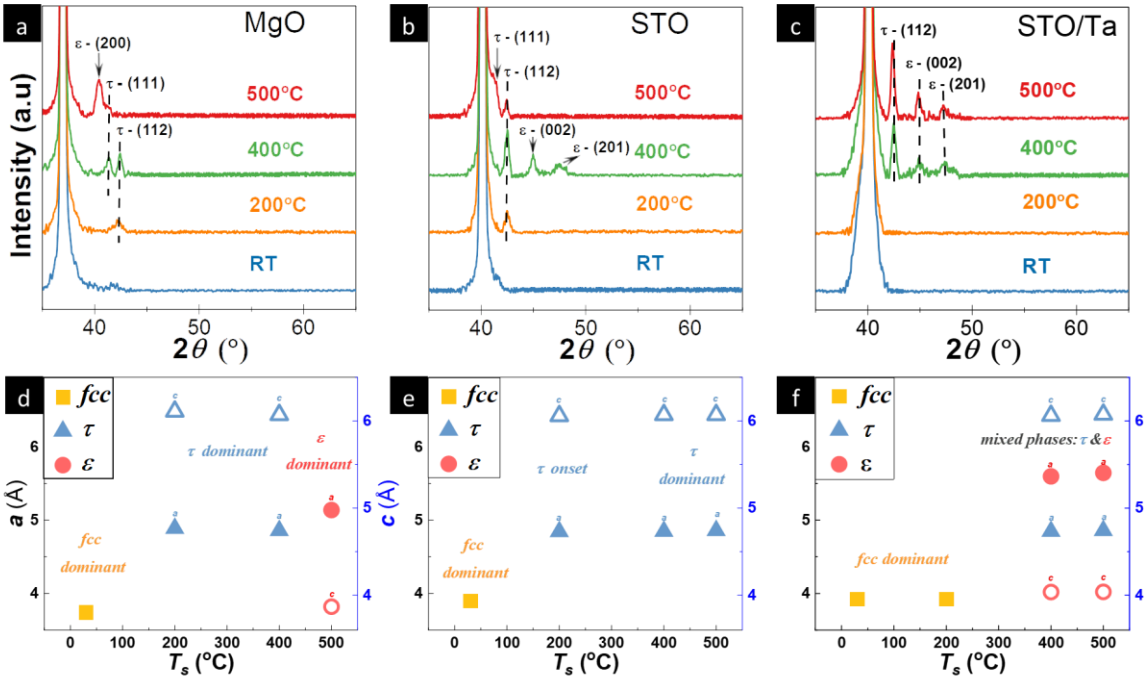

Figure 3. XRD plots of Mn3Ga on a) MgO substrate b) STO substrate and c) STO substrate with Ta at RT, 200 ºC, 400 ºC and 500 ºC and their corresponding lattice parameters.

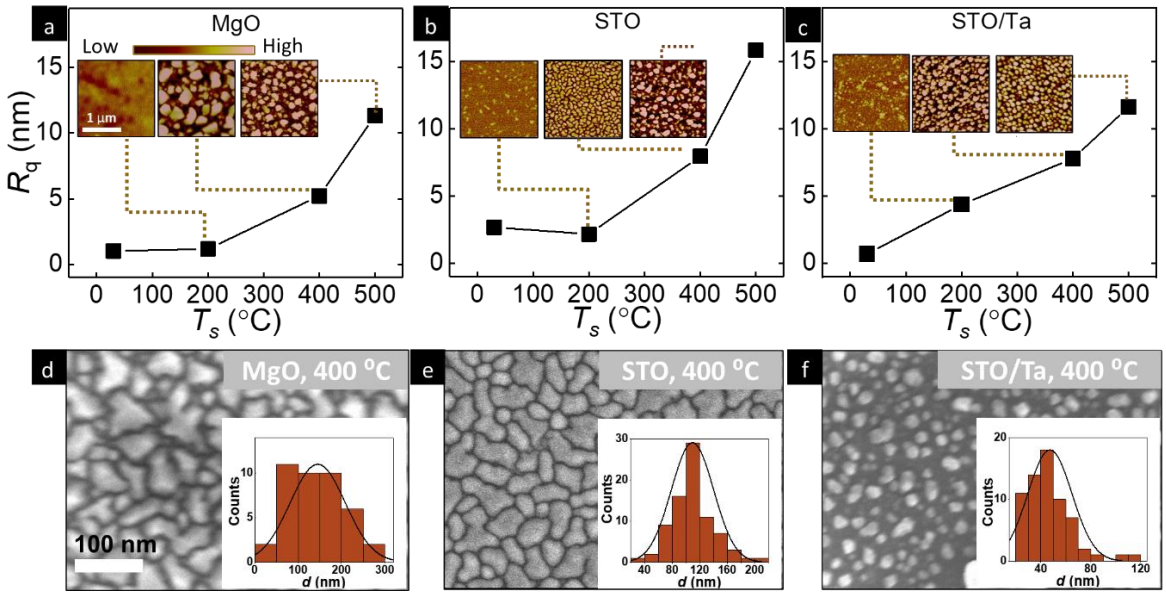

Figure 4. Roughness of Mn_3Ga thin films on a) MgO substrate b) STO substrate and c) STO substrate with Ta buffer layer at T_s of RT, 200 ºC, 400 ºC and 500 ºC

Acknowledgement

This research is supported by A*STAR Project No. C210812017.

AUTHOR DECLARATIONS

Conflict of Interest

The authors declare that they have no conflicts of interest.

References

1. H.-W. Bang, W. Yoo, C. Kim, S. Lee, J. Gu, Y. Park, K. Lee and M.-H. Jung, *Structural, magnetic, and electrical properties of collinear antiferromagnetic heteroepitaxy cubic Mn3Ga thin films*, Applied Physics Letters **115** (1), 012402 (2019).

2. F. Hu, G. Xu, Y. You, Z. Zhang, Z. Xu, Y. Gong, E. Liu, H. Zhang, E. Liu, W. Wang and F. Xu, *Tunable magnetic and transport properties of Mn3Ga thin films on Ta/Ru seed layer*, Journal of Applied Physics **123** (10), 103902 (2018).

3. L. Song, W. Li, S. Lv, X. Xi, D. Zhao, J. He and W. Wang, *Tuning the structural, magnetic, and transport properties of Mn3Ga alloys*, Journal of Applied Physics **131** (17), 173903 (2022).

4. H. Wu, I. Sudoh, R. Xu, W. Si, C. A. F. Vaz, J.-y. Kim, G. Vallejo-Fernandez and A. Hirohata, *Large exchange bias induced by polycrystalline Mn3Ga antiferromagnetic films with controlled layer thickness*, Journal of Physics D: Applied Physics **51** (21), 215003 (2018).

5. R. M. Gutiérrez-Pérez, J. T. Holguín-Momaca, J. T. Elizalde-Galindo, F. Espinosa-Magaña and S. F. Olive-Méndez, *Giant magnetization on Mn3Ga ultra-thin films grown by magnetron sputtering on SiO2/Si(001)*, Journal of Applied Physics **117** (12), 123902 (2015).

6. G.Florio, *Structural features of magnetic materials*, Encyclopedia of Smart Materials **5**, 1-9 (2022).

7. P. Qin, H. Yan, X. Wang, H. Chen, Z. Meng, J. Dong, M. Zhu, J. Cai, Z. Feng, X. Zhou, L. Liu, T. Zhang, Z. Zeng, J. Zhang, C. Jiang and Z. Liu, *Room-temperature magnetoresistance in an all-antiferromagnetic tunnel junction*, Nature **613** (7944), 485-489 (2023).

8. X. Chen, T. Higo, K. Tanaka, T. Nomoto, H. Tsai, H. Idzuchi, M. Shiga, S. Sakamoto, R. Ando, H. Kosaki, T. Matsuo, D. Nishio-Hamane, R. Arita, S. Miwa and S. Nakatsuji, *Octupole-driven magnetoresistance in an antiferromagnetic tunnel junction*, Nature **613** (7944), 490-495 (2023).

9. Z. Zhao, K. Zhang, Q. Guo and Y. Jiang, *Strain-dependent magnetism and anomalous Hall effect in noncollinear antiferromagnetic Mn3Pt films*, Physica E: Low-dimensional Systems and Nanostructures **138,** 115141 (2022).

10. Z. H. Liu, Y. J. Zhang, G. D. Liu, B. Ding, E. K. Liu, H. M. Jafri, Z. P. Hou, W. H. Wang, X. Q. Ma and G. H. Wu, *Transition from Anomalous Hall Effect to Topological Hall Effect in Hexagonal Non-Collinear Magnet Mn(3)Ga*, Sci Rep **7** (1), 515 (2017).

11. L. Song, B. Ding, H. Li, S. Lv, Y. Yao, D. Zhao, J. He and W. Wang, *Observation of large exchange bias above room temperature in antiferromagnetic hexagonal Mn3Ga*, Journal of Magnetism and Magnetic Materials **536,** 168109 (2021).

12. H. Kurt, K. Rode, M. Venkatesan, P. Stamenov and J. M. D. Coey, *High spin polarization in epitaxial films of ferrimagnetic Mn3Ga*, Physical Review B **83** (2),020405 (2011).

13. B. E. Zuniga-Cespedes, K. Manna, H. M. L. Noad, P.-Y. Yang, M. Nicklas, C. Felser, A. P. Mackenzie and C. W. Hicks, *Observation of an anomalous Hall effect in single-crystal Mn3Pt*, New Journal of Physics **25** (2), 023029 (2023).

14. Z. Q. Liu, H. Chen, J. M. Wang, J. H. Liu, K. Wang, Z. X. Feng, H. Yan, X. R. Wang, C. B. Jiang, J. M. D. Coey and A. H. MacDonald, *Electrical switching of the topological anomalous Hall effect in a non-collinear antiferromagnet above room temperature*, Nature Electronics **1** (3), 172-177 (2018).

15. H. Iwaki, M. Kimata, T. Ikebuchi, Y. Kobayashi, K. Oda, Y. Shiota, T. Ono and T. Moriyama, *Large anomalous Hall effect in L12-ordered antiferromagnetic Mn3Ir thin films*, Applied Physics Letters **116** (2), 022408 (2020).

16. T. Chen, T. Tomita, S. Minami, M. Fu, T. Koretsune, M. Kitatani, I. Muhammad, D. Nishio-Hamane, R. Ishii, F. Ishii, R. Arita and S. Nakatsuji, *Anomalous transport due to Weyl fermions in the chiral antiferromagnets Mn(3)X, X = Sn, Ge*, Nat Commun **12** (1), 572 (2021).

17. X. Li, J. Koo, Z. Zhu, K. Behnia and B. Yan, *Field-linear anomalous Hall effect and Berry curvature induced by spin chirality in the kagome antiferromagnet Mn(3)Sn*, Nat Commun **14** (1), 1642 (2023).

18. Y. Zhang, Y. Sun, H. Yang, J. Železný, S. P. P. Parkin, C. Felser and B. Yan, *Strong anisotropic anomalous Hall effect and spin Hall effect in the chiral antiferromagnetic compoundsMn3X(X=Ge, Sn, Ga, Ir, Rh, and Pt)*, Physical Review B **95** (7), 075128 (2017).

19. X. Wang, C. Zhang, Q. Yang, L. Liu, D. Pan, X. Chen, J. Deng, T. Zhai and H.-X. Deng, *Manipulation of crystalline structure, magnetic performance, and topological feature in Mn3Ge films*, APL Materials **9** (11), 111107 (2021).

20. H.-W. Bang, W. Yoo, K. Lee, Y. H. Lee and M.-H. Jung, *Magnetic and structural phase transitions by annealing in tetragonal and cubic Mn3Ga thin films*, Journal of Alloys and Compounds **869**, 159346 (2021).

21. J. T. Holguín-Momaca, C. J. Muñoz-Carnero, H. Sharma, C. R. Santillán-Rodríguez, J. A. Matutes-Aquino, C. V. Tomy and S. F. Olive-Méndez, *Tuning the ferromagnetism of epitaxial-strained D019-Mn3Ga thin films*, Journal of Magnetism and Magnetic Materials **471**, 329-333 (2019).

22. L. Šmejkal, A. H. MacDonald, J. Sinova, S. Nakatsuji and T. Jungwirth, *Anomalous Hall antiferromagnets*, Nature Reviews Materials **7** (6), 482-496 (2022).

23. S. Chen, J. X. D. Lin, B. C. Lim, H. K. Tan, Y. Y. K. Hnin, S. K. Wong, I. Lim, R. J. J. Lim., K. H. Khoo and P. Ho, *Private Commun,1*. (2023).

24. T. M. Ahn, *Nucleation Kinetics of Crystalline Ordering in Alloy 600 at Elevated Temperature for Study of Stress Corrosion Cracking*. Nuclear Regulatory Commission (2018).